

Tsunami impact to Washington and northern Oregon from segment ruptures on the southern Cascadia subduction zone

George R. Priest · Yinglong Zhang · Robert C. Witter ·
Kelin Wang · Chris Goldfinger · Laura Stimely

Received: 30 May 2013 / Accepted: 7 January 2014 / Published online: 18 January 2014
© US Government 2014

Abstract This paper explores the size and arrival of tsunamis in Oregon and Washington from the most likely partial ruptures of the Cascadia subduction zone (CSZ) in order to determine (1) how quickly tsunami height declines away from sources, (2) evacuation time before significant inundation, and (3) extent of felt shaking that would trigger evacuation. According to interpretations of offshore turbidite deposits, the most frequent partial ruptures are of the southern CSZ. Combined recurrence of ruptures extending ~490 km from Cape Mendocino, California, to Waldport, Oregon (segment C) and ~320 km from Cape Mendocino to Cape Blanco, Oregon (segment D), is ~530 years. This recurrence is similar to frequency of full-margin ruptures on the CSZ inferred from paleoseismic data and to frequency of the largest distant tsunami sources threatening Washington and Oregon, ~ M_w 9.2 earthquakes from the Gulf of Alaska. Simulated segment C and D ruptures

Some data from this paper has been presented at informal talks to the public.

Electronic supplementary material The online version of this article (doi:[10.1007/s11069-014-1041-7](https://doi.org/10.1007/s11069-014-1041-7)) contains supplementary material, which is available to authorized users.

G. R. Priest (✉) · L. Stimely
Oregon Department of Geology and Mineral Industries, Newport Coastal Field Office, Newport, OR,
USA

e-mail: george.priest@dogami.state.or.us

URL: <http://www.oregon.gov/DOGAMI/FIELDOFFICES/fieldoffice.shtml>

L. Stimely

e-mail: laura.stimelyr@dogami.state.us.or

Y. Zhang

Center for Coastal Resources Management, Virginia Institute of Marine Science, Gloucester Point,
VA, USA

e-mail: yjzhang@vims.edu

URL: http://www.vims.edu/about/directory/faculty/zhang_yj.php

R. C. Witter

U.S. Geological Survey, Alaska Science Center, Anchorage, AK, USA

e-mail: rwitter@usgs.gov

produce relatively low-amplitude tsunamis north of source areas, even for extreme (20 m) peak slip on segment C. More than ~ 70 km north of segments C and D, the first tsunami arrival at the 10-m water depth has an amplitude of <1.9 m. The largest waves are trapped edge waves with amplitude ≤ 4.2 m that arrive ≥ 2 h after the earthquake. MM V–VI shaking could trigger evacuation of educated populaces as far north as Newport, Oregon for segment D events and Grays Harbor, Washington for segment C events. The NOAA and local warning systems will be the only warning at greater distances from sources.

Keywords Tsunami · Cascadia · Segment ruptures · Warning · Earthquake

Abbreviations

DOGAMI	Oregon Department of Geology and Mineral Industries
CSZ	Cascadia subduction zone
MHHW	Mean higher high water
NOAA	National Oceanic and Atmospheric Administration

1 Introduction

While it is well known that the large height and short time of arrival of tsunamis generated by full-margin ruptures of the Cascadia subduction zone (CSZ) pose a major threat to coastal communities in Oregon, Washington, and British Columbia (e.g., Atwater et al. 1995, 2005; Dragert and Hyndman 1995; Satake et al. 2003; Nelson et al. 2006; Priest et al. 2009, 2010; Witter et al. 2011), the threat from partial ruptures of the southern CSZ has only recently been fully documented (Goldfinger et al. 2012). Evidence supporting a ~ 500 -year average recurrence interval for great tsunamis comes from the 10,000-year record of offshore turbidites (Goldfinger et al. 2012) that are inferred to be the deposits of turbidity currents triggered by tsunamigenic Cascadia earthquakes. In addition to evidence for 19 full-margin ($>1,000$ -km-long) ruptures of the megathrust, Goldfinger et al. (2012) also interpreted turbidites deposited offshore southern Cascadia as evidence for 22 shorter ruptures extending 300–500 km north from the southern end of the CSZ at Cape Mendocino (Fig. 1). From the southern Cascadia turbidite evidence, Goldfinger et al. (2012) infer that 11 earthquakes ruptured ~ 490 km of the megathrust (segment C) and 8 earthquakes ruptured ~ 320 km of the megathrust (segment D) (Fig. 1). The average recurrence of segment C and D ruptures, ~ 530 years, is thus similar to the average recurrence of full-margin events. This recurrence and the inferred segment ruptures are also consistent with observations at Bradley Lake where tsunami deposits record Cascadia tsunamis that were able to breach a persistent ~ 6 -m barrier over the last 4,600 years (Witter et al. 2012). It

K. Wang

Geological Survey of Canada, Pacific Geoscience Centre, Sidney, BC, Canada

e-mail: kwang@nrcan-rncan.gc.ca

URL: http://www.cgc.nrcan.gc.ca/dir/index_e.php?id=8400

C. Goldfinger

Oregon State University, Corvallis, OR, USA

e-mail: gold@oce.orst.edu

URL: <http://www.coas.oregonstate.edu/>

[index.cfm?fuseaction=content.search&searchtype=people&detail=1&id=540](http://www.coas.oregonstate.edu/index.cfm?fuseaction=content.search&searchtype=people&detail=1&id=540)

will be shown that segment-sourced tsunami wave heights of this investigation are consistent with the observations at Bradley Lake.

The objective of this paper is to better understand potential impacts of tsunamis in Oregon and Washington north of hypothetical ruptures of the southern Cascadia subduction zone. Key questions that will be addressed are the following:

1. How quickly does tsunami wave height decline north of segment C and D rupture areas?
2. How much time do communities north of segment C and D rupture areas have to evacuate before the first inundation and the largest inundation occur?
3. How far north of segment C and D rupture areas will felt shaking likely trigger evacuation of a populace trained to evacuate for a local earthquake?

2 Previous work

Cherniawsky et al. (2007) simulated tsunami wave elevations and currents on Vancouver Island from one full-margin CSZ rupture and two shorter segment ruptures named by Satake et al. (2003): (a) long-narrow, (b) short-north and (c) short-south. Most relevant to this study is the short-south source that extends 440 km northward from Cape Mendocino at 40.5°N–44.3°N, roughly equivalent to segment C (Fig. 1). The short-south model used a 500-year slip deficit, producing 19-m slip in the full-slip zone of the megathrust. The model linearly decreased the slip to zero halfway through a landward transition zone from fully locked to stable sliding.

Cherniawsky et al. (2007) found that most wave energy flux from the short-south source was directed east and west. The narrow ends of the source produced low-amplitude semi-circular waves that moved north and northwest, arriving at the Juan de Fuca Strait 1 h and 20 min after the earthquake. The long sides of the source produced trapped edge waves that moved north and arrived later, although no detailed time histories were given for the US coast. Maximum wave elevations for the short-south scenario were on the order of ~ 1 m for most of the Oregon and Washington coast, but this estimate is based on a structured computational grid with relatively coarse spacing of $1,530 \times 1,100$ m. Relative to more refined grids, coarse grids such as this can have significant error for estimation of tsunami elevation and inundation (Myers and Baptista 2001).

3 Methods

3.1 Cascadia earthquake sources

The CSZ segment ruptures for this study simulate segments C and D postulated by Goldfinger et al. (2012) (Fig. 1). Modeled rupture lengths extend north from just north of Cape Mendocino at 40.4°N to near Cape Blanco at 42.75°N (segment D) and to 44.5°N at Newport, Oregon (segment C) (Fig. 1). Each segment boundary is roughly centered between the north and south limits of uncertainty of the boundary from the Goldfinger et al. (2012) turbidite data; this uncertainty is illustrated in Fig. 1 by the difference between the red slip patches and the dashed lines. Slip was then tapered smoothly to zero at the maximum limit of north–south positional uncertainty.

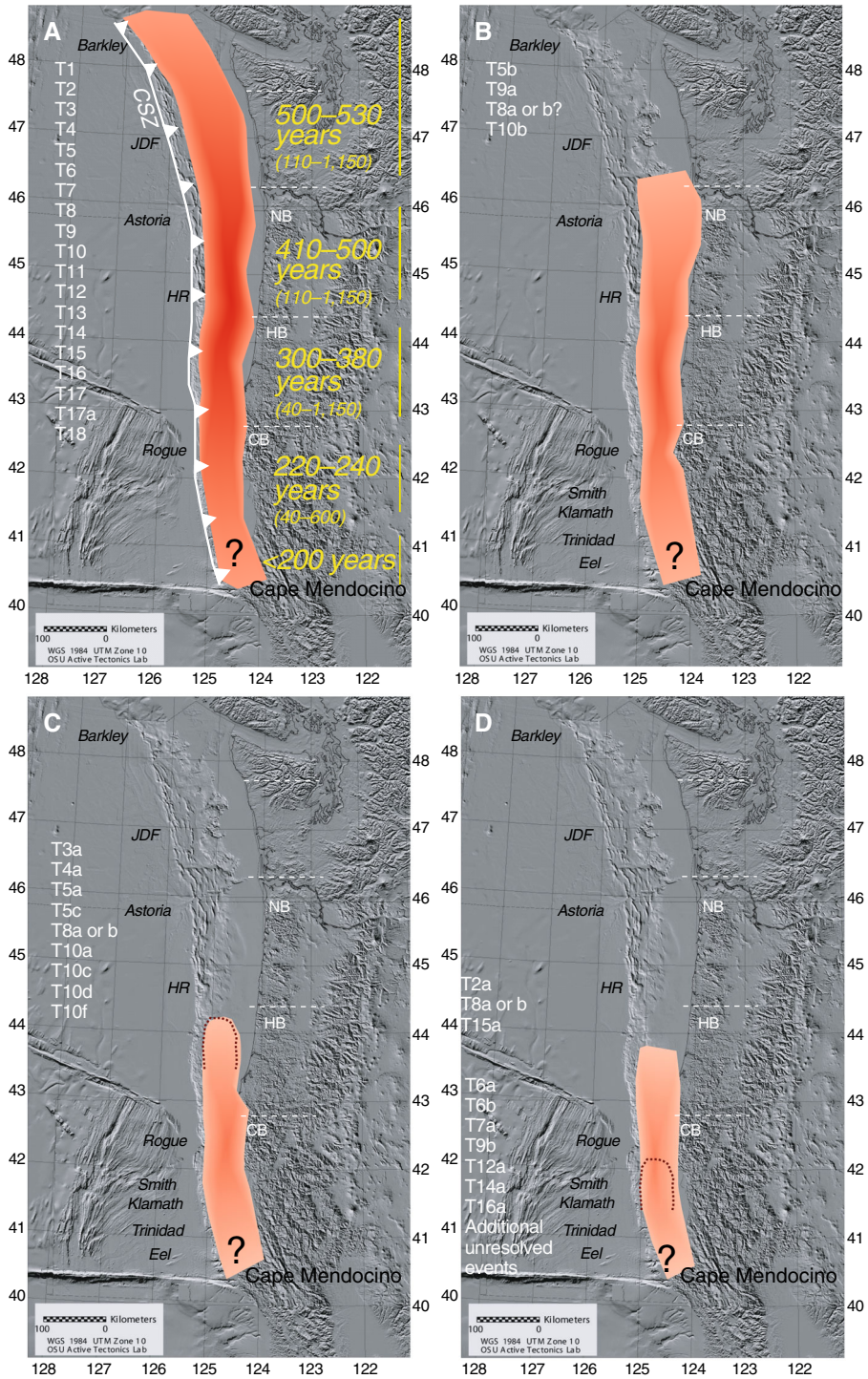


Fig. 1 Red areas depict hypothetical rupture patches of Cascadia subduction zone (CSZ) earthquakes over the last ~ 10,000 years inferred by Goldfinger et al. (2012) from marine and onshore paleoseismic data plus geological and geophysical data. White line with triangles marks the CSZ deformation front also visible as boundary between smooth to rough terrain. Numbers with “T” prefixes are offshore turbidite layers correlated with each rupture patch and arranged with youngest at the top. White dashed lines are inferred segment boundaries of CSZ ruptures designated segments A (full-margin rupture), B [rupture north to Nehalem Bank (NB)], C [rupture north to Heceta Bank (HB)], and D [rupture north to Coquille Bank (CB)]. Northern extents of segment D events break into two groups, one terminating south of the Rogue submarine canyon, indicated by dashed line. The second group extends north of Rogue but is not observed at Hydrate Ridge (HR). Although presumed to extend no further south than the southern terminus of the CSZ at Cape Mendocino, southern rupture limits are poorly known for all events indicated by query, limited by temporal coverage of turbidites and probable non-seismic turbidites in the early Holocene. Uncertainty in the northern extent of segments C and D are shown as the difference between the red patches and the black dashed lines. In the map of segment A, mean return in years of CSZ earthquakes is listed at each latitude and is calculated by dividing the number of turbidite layers into 10,000 years; minimum and maximum time intervals between turbidites at each latitude is given in parentheses. Modified from Goldfinger et al. (2012)

Coseismic vertical surface deformation was simulated by integrating the point source dislocation solution of Okada (1985) over the megathrust geometry of Witter et al. (2011). Slip direction of the coseismic rupture is assumed to be exactly opposite of plate convergence. Slip thus varies with latitude according to the plate convergence direction and rate calculated from Euler vectors as explained in Wang et al. (2003). Fault rupture models use the symmetrical down-dip slip distribution ($q = 0.5$) of Freund and Barnett (1976) modified by Wang and He (2008) with equations given in Wang et al. (2013). This slip distribution places peak slip near the continental shelf-slope break and tapers slip to zero up dip and down dip. Peak slip is calculated as the product of the recurrence interval and the local plate convergence rate based on the assumption that seismic coupling coefficient equals 1.0 at the peak of the slip distribution. The down-dip limit of slip is the same localities specified in Witter et al. (2011) and is constrained by earlier thermal modeling, horizontal GPS measurements, and geological data; the up-dip limit is at the surface trace of the CSZ and is based on the assumption of velocity strengthening behavior of the shallowest part of the megathrust beneath the outer accretionary wedge (Wang and Hu 2006; Priest et al. 2010; Witter et al. 2011).

Tsunamis from three earthquakes were simulated: segment C using a slip deficit of 400 and 588 years (sources C400 and C588, Table 1) and segment D using a slip deficit of 200 years (source D200, Table 1). Slip deficits of 400 and 200 years approximate the mean recurrence intervals of segment C and D ruptures, respectively, as inferred from turbidite

Table 1 Source parameters

Rupture scenario	Length (km)	Width (km) ^a	Interevent time (years)	Peak slip (m) ^b	Mean slip (m) ^c	Seismic moment (10 ²² N m) ^d	Moment magnitude (M_w) ^e
C588	490	66	588	20.0	10	1.27	8.7
C400	490	66	400	13.6	7	0.86	8.6
D200	320	61	200	6.8	3	0.26	8.2

^a Mean rupture width is calculated by dividing total rupture area by the listed rupture length

^b Maximum slip estimates are the product of the recurrence interval times a convergence rate at southern Oregon latitudes (34 mm year⁻¹)

^c Average slip estimate is 0.49 of maximum slip estimate

^d Seismic moment (M_0) = fault area × slip × rigidity, where rigidity = 4×10^{10} N m⁻²

^e Moment magnitude (M_w) = (log M_0 - 9.1)/1.5

paleoseismology (Goldfinger et al. 2012). A slip deficit of 588 years produces a peak slip of ~ 20 m, which represents a maximum scenario analogous to the peak slip of the 2010 M_w 8.8 Maule, Chile earthquake (Delouis et al. 2010). The C400 and D200 models use peak slips of 13.6 m and 6.8 m, respectively. Estimated moment magnitudes range from M_w 8.2 to 8.7 (Table 1). These magnitudes fall between empirical estimates based on linear regressions through modern seismic data of Blaser et al. (2010). Using their preferred oceanic thrust (subduction zone) data, the inferred M_w from rupture width would be 7.9 for D200 and 8.0 for C400 and C588; M_w for rupture length is 8.6 for D200 and 8.9 for C400 and C588.

3.2 Tsunami simulation

Vertical components of deformation from the three earthquake sources were used to set up the initial water surface for tsunami simulations, assuming a short (10 s) initial constant acceleration of the seafloor. Tsunami simulations used the hydrodynamic finite element model SELFE (Semi-implicit Eulerian–Lagrangian Finite Element model) (Zhang and Baptista 2008; Zhang et al. 2011). Algorithms used to solve the Navier–Stokes equations in this model are computationally efficient and stable. SELFE passed all standard tsunami benchmark tests (Zhang and Baptista 2008; Zhang 2012) and closely reproduced observed inundation and flow depths of the 1964 Alaska tsunami in a trial at Cannon Beach (Priest et al. 2010).

The unstructured finite element mesh was constructed by first compiling a digital elevation model (DEM) covering the project area and then retrieving from the DEM elevations at a series of points defining a triangular irregular network (TIN). The DEM for the regional simulations was compiled from the ETOPO1 1-arc-minute database (<http://www.ngdc.noaa.gov/mgg/global/global.html>) of the National Geophysical Data Center supplemented in areas of dry land by 2009 Light Detection and Ranging (LIDAR) data. All data sets were adjusted to the North American Vertical Datum of 1988 (NAVD 88) (Zilkoski et al. 1992) and WGS 84 map projection. Grid spacing for the regional simulations varied from ~ 3 to 5 km at the source to 50–70 m at the open coastal shoreline. The coastal boundary simulates inland inundation by using fine resolution near the shoreline and dry land (e.g., up to 100 m above assumed tide) and coarser resolution in the case of extreme runup further inland. Each regional Cascadia simulation was run for 6 h of “tsunami time.”

All simulations were run at mean higher high water (MHHW) at the Port Orford, Oregon tide gauge in southern Oregon, 2.07 m NAVD 1988; this value approximates the mean high water (MHW) tidal level for northern Oregon and Washington, which lies about 0.2–0.3 m below MHHW. All simulations used a Manning Coefficient of zero (i.e., zero bottom friction). Zero friction was assumed to add conservatism to hazard estimates by minimizing tsunami travel times and maximizing wave height. Time histories for wave elevations at water depths of 50 and 10 m were extracted approximately every 50 km along the US coastline, although spacing was varied somewhat from 50 km to coincide with major population centers (Fig. 2). Positive sea-level change above this MHHW tide is here defined as the tsunami amplitude.

3.3 Extent of felt earthquake shaking

It is beyond the scope of this investigation to fully explore attenuation of seismic shaking for the modeled CSZ events, so representative modern analogues to segment C and D

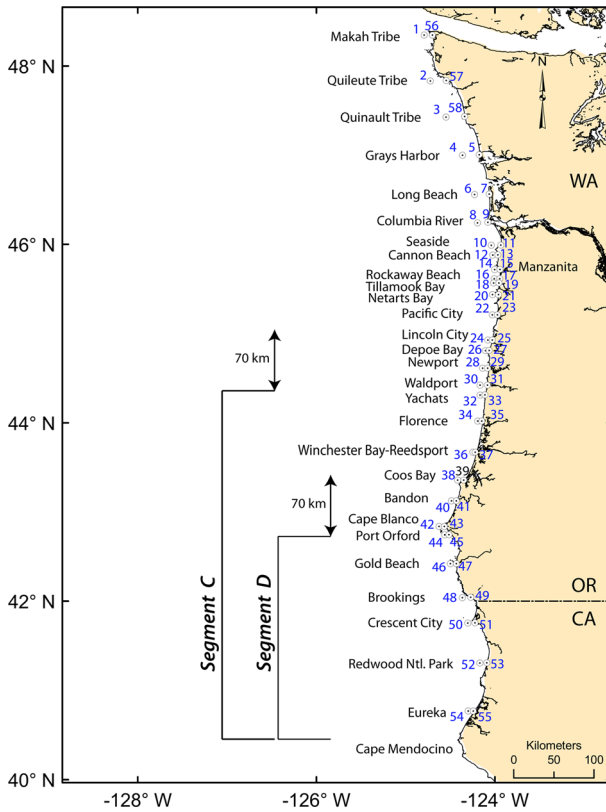


Fig. 2 Location of time history stations relative to northern and southern boundaries of CSZ segments C and D from Fig. 1. In each pair of stations, the west station is at ~50 m depth and the east station is at ~10 m depth. Tables 2 and 3 provide arrival time and height information for the stations at ~10 m depth

ruptures will be used to determine approximate extent of felt shaking intensity from the Modified Mercalli (MM) intensities listed on standard US Geological Survey Shakemaps. The Maule, Chile, 2010 earthquake will be taken as representative of segment C, and the M_w 8.4 Arequipa, Peru, earthquake will be the segment D analogue. Rupture length and magnitude of these events are similar to the corresponding segment scenarios: Maule with M_w of 8.8 and length of ~430 km (US Geological Survey 2010) versus 490 km and M_w 8.6–8.7 for segment C, and Arequipa with length of ~280-km and M_w of 8.4 (US Geological Survey 2001) versus 320 km and M_w 8.2 for segment D (Table 1).

4 Results

4.1 Cascadia earthquake deformation model

Maximum coseismic uplift from the two Cascadia source scenarios was 5 m for C588 (Fig. 3), 3.5 m for C400 (Fig. 4), and 1.7 m for D200 (Fig. 5). Maximum coseismic subsidence was 3.6 m for C588, 2.5 m for C400, and 1.2 m for D200.

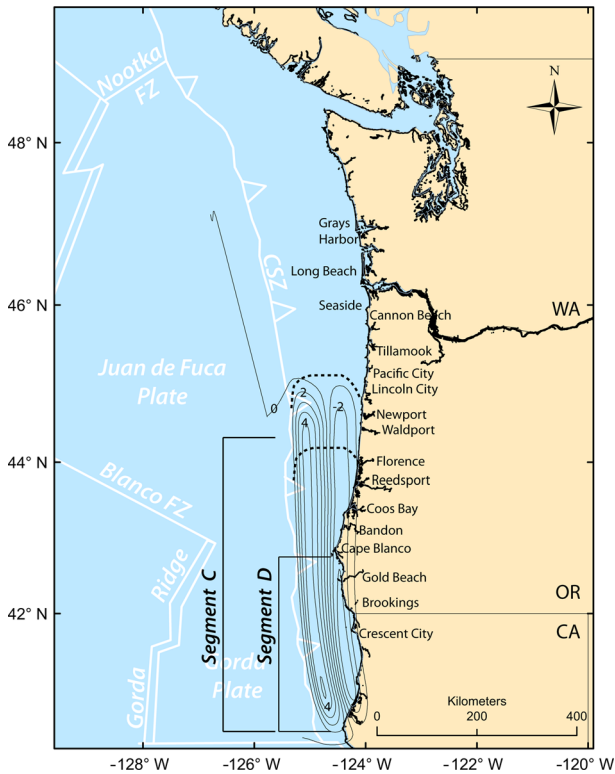


Fig. 3 C588 vertical coseismic deformation (1-m contours); positive numbers = uplift; negative numbers = subsidence. *Bold dashed lines* are north and south limits of uncertainty in location of northern boundary of Segment C from Goldfinger et al. (2012). Segment boundaries are those of Fig. 1

4.2 Tsunami wave amplitude

Due to the offshore patterns of subsidence for all sources (Figs. 3, 4, 5), time histories of wave arrivals exhibit small leading depression waves north and south of Cape Blanco (Figs. 6 and 7). But the most important phenomenon is the sharp decline in maximum amplitude north of each source (Fig. 8; Tables 2 and 3). It is clear from the time histories at the ~ 10 -m isobath that maximum tsunami wave amplitudes >70 km north of source areas were not from the initial arrival but from later refracted edge waves traveling from the source areas (Figs. 6, 7). At >70 km north of the sources, amplitudes of initial tsunami arrivals are <1 m for segment C sources and <0.3 m for the segment D source (Figs. 6, 7; Tables 2 and 3), and peak arrivals were ≤ 4.2 m for segment D and $\leq \sim 1$ m for segment C (Figs. 6, 7, 8; Tables 2 and 3). Reversal of the trend toward decreasing amplitude north of sources occurred at Long Beach, Washington and Seaside, Oregon from probable bathymetric amplification (Fig. 8; Table 2).

The peak arrivals more than 70 km north of the source generally occurred more than 2 h after the earthquakes (Figs. 6, 7; Tables 2 and 3). The variations at 0–70 km from the source are illustrated by the southern three time histories in Figs. 6 and 7; from south to north, these illustrate: (1) tsunami amplitudes at the source (Gold Beach), (2) the closest point to the source where the first arrival is approximately half that of the source (i.e., Lincoln City for C400 and C588 and Bandon for D200), and (3) the closest point to the source where the first

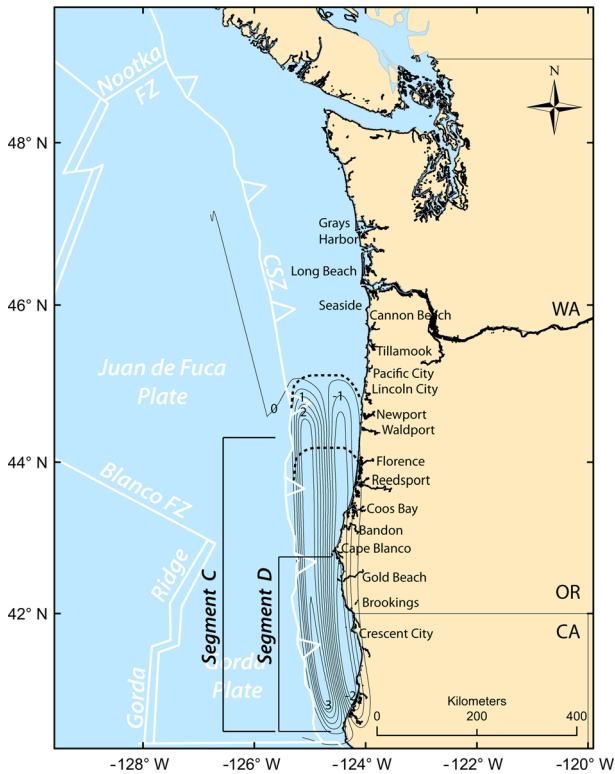


Fig. 4 C400 vertical coseismic deformation (0.5-m contours); positive numbers = uplift; negative numbers = subsidence. *Bold dashed lines* are north and south limits of uncertainty in location of northern boundary of segment C from Goldfinger et al. (2012)

arrival is less than later arrivals (i.e., Pacific City for C400 and C588 and the Winchester Bay area for D200). The latter occurs only 70 km north of the sources where the first arrival is ≤ 1.9 m for segment C sources and 0.2 m for the segment D source. At these same observation points 70 km north of sources, maximum amplitudes of later arriving edge waves are ≤ 3.6 m for the segment C sources and 0.4 m for the segment D source, but these peak values are reached at ~ 2.8 h after the earthquake for the former and ~ 1.6 h for the latter (Figs. 6, 7; Tables 2, 3). Initial arrivals reached the northernmost Washington coast ~ 150 km north of Grays Harbor 1.4 and 1.7 h after the segment C and D earthquakes, respectively (Figs. 6, 7; Tables 2, 3); thus, mean velocities of the initial arrivals were on the order of 310–370 km/h.

Maximum tsunami wave amplitudes retrieved from the 50-m and 10-m isobaths are available in digital file `Max_tsunami_elevations_Priest_et_al.xlsx`. Time history locations and data retrieved from these same isobaths are available in digital file `Time_histories_Priest_et_al.xlsx`.

5 Discussion

5.1 Key findings

Tsunami simulations for hypothetical ruptures of southern segments of the CSZ, segments C and D (Fig. 1) predict maximum open coastal wave amplitudes at 10-m water depth of

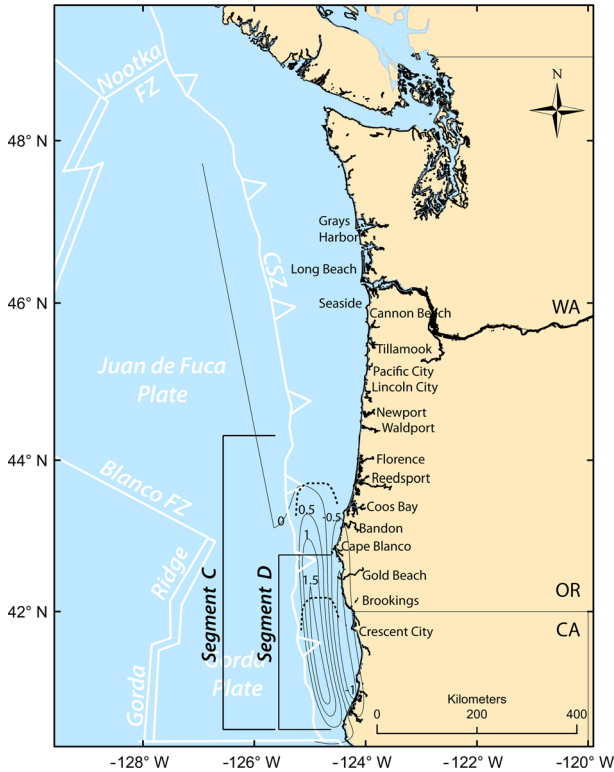


Fig. 5 D200 vertical coseismic deformation (0.5-m contours); positive numbers = uplift; negative numbers = subsidence. **Bold dashed lines** are north and south limits of uncertainty in location of northern boundary of segment D from Goldfinger et al. (2012). Segment boundaries are those of Fig. 1

≤ 4.2 m at >70 km north of segment ruptures (Figs. 6, 7, 8), even for an extreme earthquake (M_w 8.7) with peak slip of 20 m on segment C (C588, Fig. 8). Detailed simulations of tsunami inundation in the Bandon, Oregon area (Witter et al. 2011) show that wave amplitudes at 10-m water depth of this study are generally amplified by ~ 10 percent at the shoreline (0 m); Bandon has bathymetry similar to other Pacific Northwest beaches. While tsunami amplitude generally decreases north of segment ruptures, anomalous increases in amplitude at Long Beach, Washington and Seaside, Oregon, are probably caused by local bathymetric amplification (Fig. 7).

Similar to findings of Cherniawsky et al. (2007), maximum wave amplitudes more than 70 km north of the segment ruptures are not from the first tsunami arrival but from refracted edge waves striking ≥ 2 h after the earthquake (Figs. 6, 7; Tables 2, 3). Owing to the narrow width relative to length of Cascadia ruptures (high aspect ratio), most tsunami energy is directed perpendicular to the long axis of ruptures as is known from theoretical studies (see Geist (1998) for summary); thus, first arrivals more than ~ 70 km north of segment C and D ruptures have amplitudes ≤ 1.9 m but do strike the entire Oregon and Washington coast within 1.4–1.7 h of these earthquakes (Figs. 6, 7; Tables 2, 3). Slight modification of amplitude can occur from dynamic propagation of ruptures (Geist 1998), so these heights derived from static rupture models are only approximations. Splay faulting in southern Cascadia sources, probably more likely for larger slip events like C588, could

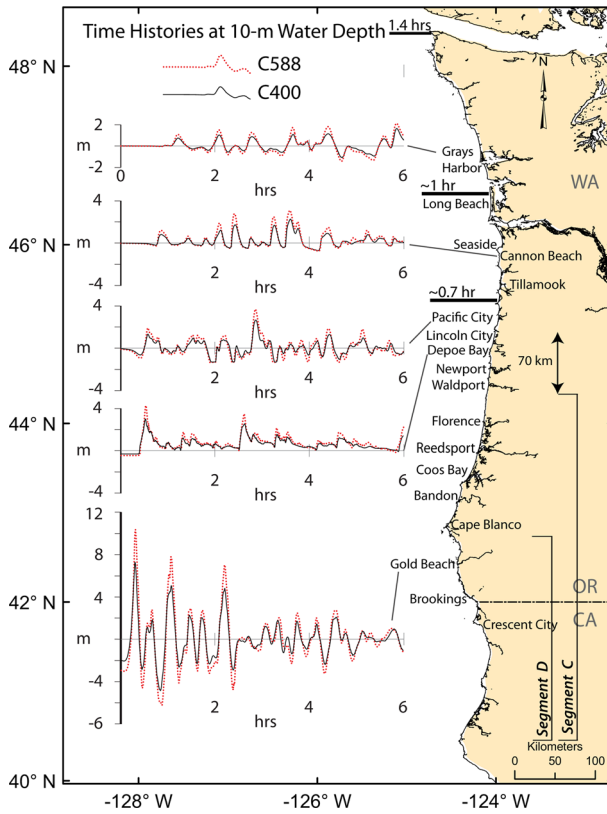


Fig. 6 C400 and C588 time histories of tsunami wave elevation relative to the MHHW model tide at approximately the 10-m water depth. **Bold labels on bold horizontal lines** refer to the time of arrival of the first tsunami wave peak at the 10-m water depth. Segment boundaries are those of Fig. 1

also amplify tsunami amplitude at the open coast by up to ~20 % for all slip partitioned to a splay fault (Witter et al. 2011). In any case, the initial arrivals are unlikely to cause inundation over widespread areas. However, the waves may endanger people on beaches and low-lying coastal areas and create strong currents in ports and harbors.

North of these two CSZ segment ruptures, the resulting tsunamis are probably not larger than the largest distant tsunamis. The largest historical distant tsunami was from the 1964 M_w 9.2 Prince William Sound earthquake that produced wave heights of 3–5 m (relative to mean high water) on the northern Oregon coast (Schatz et al. 1964), but many of these observations were from estuaries. Open coastal run-up for the 1964 tsunami was probably ~6 m NAVD88 based on detailed field observations from Seaside, Oregon (González et al. 2009) and Cannon Beach (Witter 2008). A similar but hypothetical Gulf of Alaska earthquake (Source 3 of González et al. 2009) with larger uplift and better directivity toward the Pacific Northwest coast produced maximum open coastal tsunami wave elevations ~8–9 m above MHHW tide at Cannon Beach (Priest et al. 2009, 2010) and ~4 m above tide at Bandon, Oregon (Witter et al. 2011). González et al. (2009) assigned a recurrence of 750 years to these large Gulf of Alaska tsunamis, so these extreme distant tsunamis are probably no more frequent than the combined 19 segment C and D ruptures over the last 10,000 years (recurrence of 526 years;

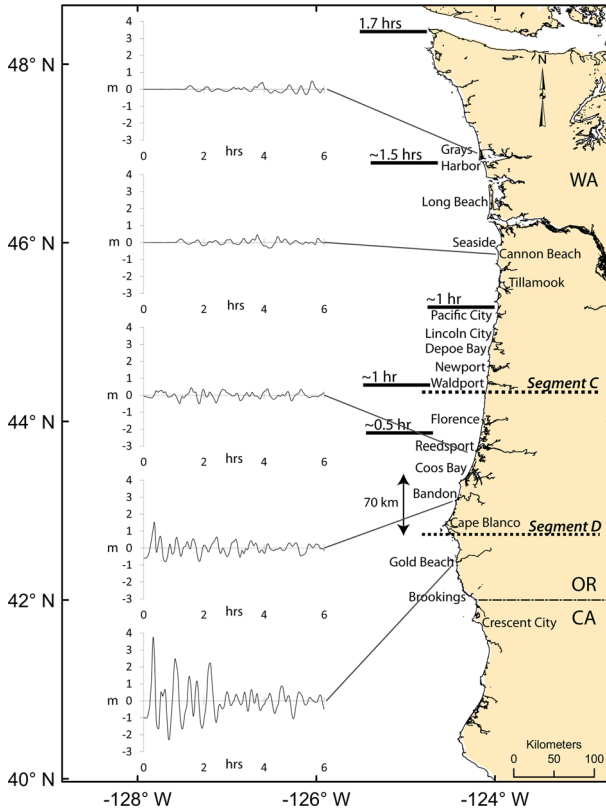


Fig. 7 D200 time histories of tsunami wave elevation relative to the MHHW model tide at approximately the 10-m water depth. **Bold labels on bold horizontal lines** refer to the time of arrival of the first tsunami wave peak at the 10-m water depth. Segment boundaries are those of Fig. 1

Fig. 1; Goldfinger et al. 2012). Interestingly, these largest distant tsunamis are also no more frequent than the 19 full-margin CSZ ruptures that occurred over the last 10,000 years (Fig. 1; Goldfinger et al. 2012).

The National Oceanic and Atmospheric Administration (NOAA) tsunami warning system and felt shaking in Oregon should trigger widespread evacuation, minimizing loss of life to tsunamis north of segment ruptures on the CSZ. The West Coast and Alaska Tsunami Warning Center normally issues warnings approximately 5 min after earthquake occurrence (West Coast and Alaska Tsunami Warning Center 2013). Earthquakes of these magnitudes would put the entire west coast into a tsunami warning, since projected wave heights would certainly exceed the 1-m threshold. The warning system should not be disabled by earthquake shaking in areas like northern Oregon and Washington that are distant from CSZ segment source areas. An extreme segment earthquake such as the C588 scenario that approximates the Maule, Chile 2010 event, would have felt shaking similar to that in Chile where Modified Mercalli (MM) intensities of V–VI (felt by almost everyone to slight damage) occurred ~250–300 km north and south of the rupture zone and felt shaking extended at least 400 km (US Geological Survey 2010). Using the M_w 8.4 Arequipa, Peru earthquake as an analogue to a segment D event (US Geological Survey 2001), MM V–VI should extend ~200 km north and south of the rupture and felt shaking

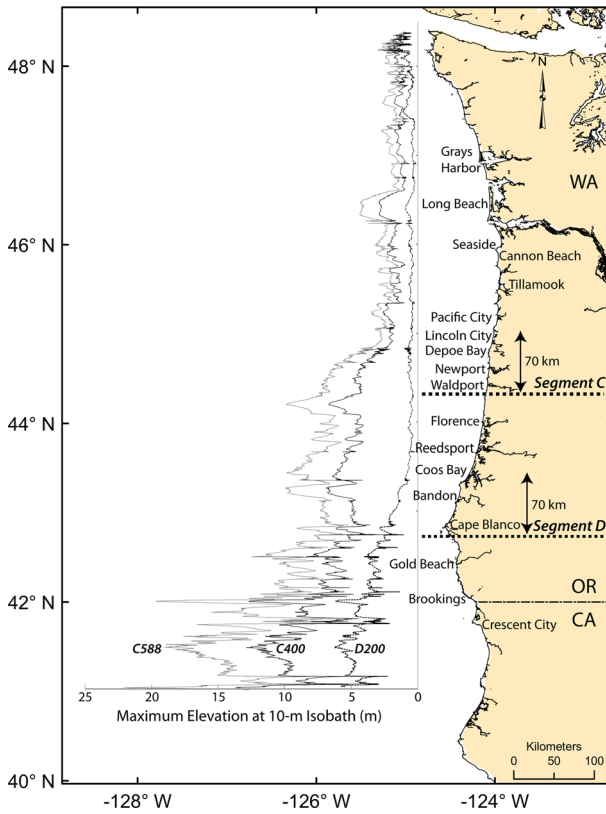


Fig. 8 Maximum tsunami amplitudes at the 10-m water depth for simulations C588 (segment C, 588 years of strain release), C400 (segment C, 400 years of strain release), and D200 (segment D, 200 years of strain release). Segment boundaries are those of Fig. 1

at least 300 km. If these earthquakes are analogous to Cascadia events, then MM V–VI shaking should extend as far north as ~Grays Harbor, Washington for extreme segment C events and to ~Newport, Oregon for segment D earthquakes. Hopefully, the felt shaking would trigger evacuation in and near source areas for a populace previously trained to evacuate in the event of a local earthquake. The National Tsunami Hazard Mitigation Program has, since 1997, supported vigorous education and outreach programs in Oregon, Washington and California to instill in local populations the meaning of NOAA tsunami warnings and the message that significant felt shaking should trigger evacuation from low-lying areas.

Previous sensitivity studies suggest that radiation of tsunami energy south of the Cascadia sources is as small as it is north. For example, Borrero (2006) demonstrated that Cascadia ruptures with mean slip of 4–20 m produced tsunami wave heights ≤ 1.4 m at the Golden Gate Bridge in San Francisco Bay (~400 km south of the CSZ).

5.2 Paleotsunami evidence at Bradley Lake

Correlations between offshore turbidites and tsunami deposits in Bradley Lake imply that ruptures of Cascadia segment D (Fig. 5) rarely produced large tsunamis (Goldfinger et al.

Table 2 Initial and peak wave arrival times and elevations (elev.) above the model tide at the 10-m isobath (see Fig. 2) for C400 and C588, arranged from north to south

No.	Geographic area	C400 initial peak arrival time (h)	C400 initial peak arrival elev. (m)	C400 largest peak arrival time (h)	C400 largest peak arrival elev. (m)	C588 initial peak arrival time (h)	C588 initial peak arrival elev. (m)	C588 largest peak arrival time (h)	C588 largest peak arrival elev. (m)
56	Makah Tribe	1.43	0.3	4.15	1.6	1.43	0.4	4.13	1.8
57	Quileute Tribe	1.25	0.5	3.71	1.2	1.25	0.8	3.72	1.7
58	Quinalt Tribe	1.22	0.4	5.78	1.5	1.22	0.7	5.74	1.8
5	Grays Harbor	1.19	0.7	5.84	1.6	1.19	1.0	5.83	2.1
7	Long Beach	1.01	0.6	3.54	2.5	1.02	0.9	3.47	3.7
9	Columbia River	0.90	0.3	4.97	1.3	0.90	0.5	4.96	2.2
11	Seaside	0.91	0.9	3.84	2.9	0.91	1.3	3.83	3.9
13	Cannon Beach	0.84	0.8	3.58	2.2	0.83	1.1	3.58	3.0
15	Manzanita	0.76	1.0	2.31	2.2	0.76	1.5	2.31	3.0
17	Rockaway	0.70	0.9	2.28	2.3	0.71	1.4	2.26	3.0
19	Tillamook Bay	0.76	0.5	2.26	1.2	0.76	0.8	2.25	1.9
21	Netarts Bay	0.68	1.3	2.25	2.6	0.68	1.9	2.19	3.6
23	Pacific City	0.56	1.2	2.84	2.6	0.56	1.9	2.84	3.6
25	Lincoln City	0.53	1.9	2.72	2.1	0.53	2.8	2.73	2.8
27	Depoe Bay	0.53	3.0	0.53	3.0	0.52	4.3	0.52	4.3
29	Newport	0.57	3.9	0.57	3.9	0.57	5.6	0.57	5.6
31	Waldport	0.66	7.4	0.66	7.4	0.62	10.2	0.62	10.2
33	Yachats	0.62	6.1	0.62	6.1	0.61	8.7	0.61	8.7
35	Florence	0.51	4.5	0.51	4.5	0.50	6.7	0.50	6.7
37	Winchester Bay	0.38	5.0	0.38	5.0	0.38	7.2	0.38	7.2
39	Coos Bay	0.34	5.8	0.34	5.8	0.34	8.4	0.34	8.4
41	Bandon	0.33	4.8	0.33	4.8	0.33	6.8	0.33	6.8
43	Cape Blanco	0.27	4.4	0.27	4.4	0.24	6.3	0.24	6.3
45	Port Orford	0.27	4.4	0.27	4.4	0.24	6.2	0.24	6.2

Table 2 continued

No.	Geographic area	C400 initial peak arrival time (h)	C400 initial peak arrival elev. (m)	C400 largest peak arrival time (h)	C400 largest peak arrival elev. (m)	C588 initial peak arrival time (h)	C588 initial peak arrival elev. (m)	C588 largest peak arrival time (h)	C588 largest peak arrival elev. (m)
47	Gold Beach	0.31	7.3	0.31	7.3	0.30	10.4	0.30	10.4
49	Brookings	0.36	7.3	0.36	7.3	0.36	10.9	0.36	10.9
51	Crescent City	0.32	6.9	0.32	6.9	0.31	9.8	0.31	9.8
53	Redwood National Park	0.36	10.2	0.36	10.2	0.35	15.1	0.35	15.1
55	Eureka	0.27	5.7	0.27	5.7	0.27	8.6	0.27	8.6

Table 3 Initial and peak wave arrival times and elevations (elev.) above model tide at the 10-m isobath (see Fig. 2) for D200, arranged from north to south

No.	Geographic area	D200 initial arrival time (h)	D200 initial arrival elev. (m)	D200 peak arrival time (h)	D200 peak arrival elev. (m)
56	Makah Tribe	1.70	0.1	4.47	1.3
57	Quileute Tribe	1.56	0.2	4.97	0.4
58	Quinalt Tribe	1.53	0.1	5.73	0.8
5	Grays Harbor	1.5	0.2	5.58	0.5
7	Long Beach	1.36	0.2	5.37	0.4
9	Columbia River	1.24	0.1	4.99	0.4
11	Seaside	1.29	0.2	3.85	0.9
13	Cannon Beach	1.21	0.2	3.76	0.4
15	Manzanita	1.13	0.2	5.64	0.5
17	Rockaway	1.1	0.2	5.56	0.6
19	Tillamook Bay	1.08	0.1	5.43	0.4
21	Netarts Bay	1.06	0.2	5.34	0.5
23	Pacific City	0.98	0.2	3	0.5
25	Lincoln City	0.93	0.2	2.73	0.5
27	Depoe Bay	0.88	0.4	3.62	0.9
29	Newport*	0.95	0.2	2.6	0.5
31	Waldport**	0.97	0.4	1.54	0.7
33	Yachats	0.87	0.7	2.14	0.8
35	Florence	0.73	0.3	3.09	0.6
37	Winchester Bay	0.40	0.2	1.56	.4
39	Coos Bay	0.36	0.9	0.36	0.9
41	Bandon	0.34	1.5	0.34	1.5
43	Cape Blanco	0.25	2.1	0.25	2.1
45	Port Orford	0.24	2.1	0.24	2.1
47	Gold Beach	0.31	3.7	0.31	3.7
49	Brookings	0.37	4.0	0.37	4.0

Table 3 continued

No.	Geographic area	D200 initial arrival time (h)	D200 initial arrival elev. (m)	D200 peak arrival time (h)	D200 peak arrival elev. (m)
51	Crescent City	0.34	3.5	0.34	3.5
53	Redwood National Park	0.37	5.3	0.37	5.3
55	Eureka	0.28	2.9	0.28	2.9

* Newport has ~0.4–0.5-m peak arrivals at 1.54, 2.59, 3.67, 4.56, and 5.95 h, owing to wave trapping by a nearby submarine bank

** Waldport has 0.5–0.7-m peak arrivals at 1.54, 2.56, 3.66, 4.13, and 5.62 h owing to wave trapping by a nearby submarine bank

2012; Witter et al. 2012). Bradley Lake is a coastal lake near the northern end of segment D, 4 km south of Bandon (Fig. 5). The lake has been in a geomorphic condition to effectively capture and preserve Cascadia tsunami-deposited sands for the last ~4,600 years over which time mean recurrence of sand layers is 380–400 years (Kelsey et al. 2005). This recurrence is essentially equal to the 300–380 years recurrence of Cascadia earthquakes estimated by Goldfinger et al. (2012) from turbidites deposited in segments A, B, and C that are directly offshore of Bradley Lake (Fig. 1, map A). If segment D tsunamis could routinely reach the lake, then tsunami deposits would have a recurrence closer to 220–240 years (Fig. 1, map A). In fact, the smallest thinnest segment D turbidites (T2a, T6a, T6b, T7a, T8a or T8b, T9b, T12a, T14a, and T16a) are not correlative with any of the Bradley Lake tsunami deposits (Goldfinger et al. 2012). These data suggest that Cascadia ruptures directly offshore of the lake caused lake inundation rather than tsunamis produced by segment D ruptures, probably because ruptures offshore would be closer and would generate more coastal subsidence (Figs. 3, 4, 5). D200 wave height above MHHW near the shoreline is only ~1.7 m at Bradley Lake and coastal subsidence ~0.7 m. Tsunami simulations by Witter et al. (2012) showed that for tsunamis to breach the 6-m lake outlet required >12–13 m (≥ 360 –400 years slip deficit) peak slip on ruptures directly offshore for the AD 1700 landscape and >8–9 m (>260 years slip deficit) for the most landward prehistoric shoreline. The 12–13 m peak slip at Bradley

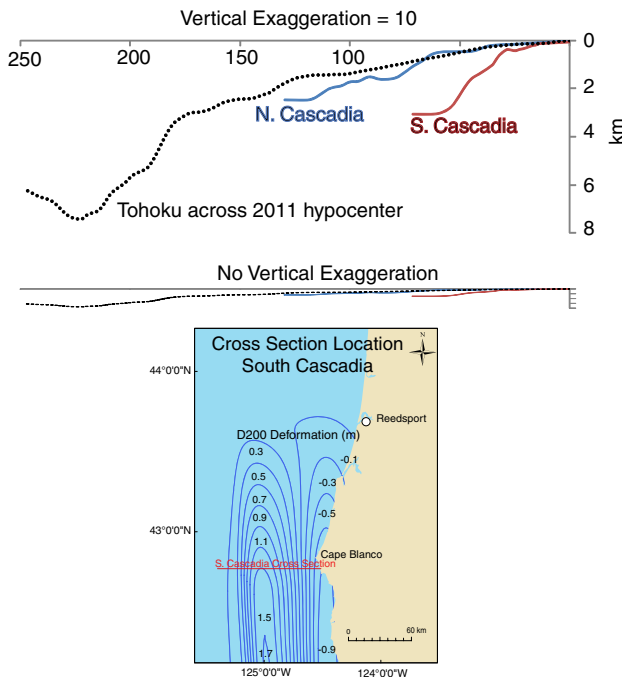


Fig. 9 Comparison of continental slope of the Japan subduction zone at the hypocenter of the March 11, 2011 Tohoku earthquake to continental slope of the northern and southern Cascadia subduction zone (upper diagrams). Lower map shows location of the southern Cascadia cross-section relative to vertical coseismic deformation (0.2-m contours) for the D200 source; northern Cascadia cross-section is at the latitude of Tillamook, Oregon (45.48°N) and shows the much lower continental slope typical of northern Oregon and Washington. The subduction zone fault reaches the ocean floor at the base of the continental slope in each cross-section

Lake also matches the preferred coseismic slip model of Wang et al. (2013) based on paleo-subsidence data from the AD 1700 Cascadia earthquake. Interestingly, AD 1700 slip patch boundaries from the Wang et al. (2013) preferred model are very similar to the segment boundaries inferred from turbidite data by Goldfinger et al. (2012). Goldfinger et al. (2012) noted that the paleoseismic segment boundaries based on offshore data, though uncertain, are also similar to those inferred by Boyarko (2010) for segmentation patterns observed in Episodic Tremor and Slip (ETS) events along strike.

5.3 Could slip extend up dip and break the seafloor?

Extreme seaward skew of slip toward the deformation front significantly amplifies tsunamis relative to the Wang and He (2008) fault model used here (Priest et al. 2010). The Wang and He (2008) model tapers slip seaward to the deformation front following the velocity strengthening model so that coseismic ruptures do not break the seafloor and coseismic slip is not skewed toward the trench, but there is some uncertainty about this assumption. It is possible that, in the course of the evolution of pore fluid pressure distribution, parts of the up-dip segment at some subduction zones may occasionally become moderately velocity-weakening, and when triggered to slip, acquire tsunamigenic rupture speed, producing “tsunami earthquakes” with relatively high slip near the deformation front, low felt shaking, and large tsunamis (Seno 2002; Wang and He 2008). While these earthquakes may be possible on the CSZ, widespread occurrence of turbidites offshore (e.g., Goldfinger et al. 2003, 2012) and liquefaction features onshore (Obermeier and Dickenson 2000) are consistent with at least moderate coseismic ground motion over wide areas for the vast majority of CSZ events.

Even if tsunami earthquakes are not common on the CSZ, this does not foreclose the possibility of “runaway slip” events such as apparently occurred during the M_w 9.0 March 11, 2011 Tohoku earthquake, whereby extreme slip (~ 50 – 60 m) and extension of the outer accretionary wedge was apparently triggered by a great earthquake farther down dip (Tsuji et al. 2013). One of the prerequisites for such extensional deformation in the outer accretionary wedge is a gravitationally unstable continental slope of $\sim 8^\circ$ (Tsuji et al. 2013), essentially the same as the slope on much of the southern Cascadia margin (Fig. 9). Although such events cannot be ruled out for full-margin $\sim M_w$ 9.0 CSZ earthquakes, they are probably less likely for segment events with much smaller magnitude and slip.

Priest et al. (2010) discussed uncertainty in the down-dip extent of coseismic ruptures for sources analogous to those of this investigation. Because the down-dip part of coseismic deformation is in either very shallow water or onshore, they found that geologically reasonable variations in down-dip extent of the rupture had little effect on the resulting tsunamis.

6 Conclusions

Segment ruptures on the southern CSZ pose a moderate threat to coastal populations more than 70 km north of source areas, primarily from late-arriving refracted waves. Initial waves arrive within 1.4–1.7 h of the earthquake along the entire Oregon and Washington coasts and are of low amplitude (≤ 1.9 m above tide), posing a danger to people on beaches and producing strong currents in boat harbors. Later, refracted edge waves more than 70 km north of segment sources are ≤ 4.2 m above tide but arrive ≥ 2 h after the

earthquake, so NOAA tsunami warnings should provide sufficient time for vulnerable populations to evacuate. Segment ruptures will produce strong shaking proximal to sources in southern Cascadia, which will be the only effective warning in southern Oregon and northern California. Shaking should also be felt north of the segment ruptures in Oregon as far north as Newport, Oregon for segment D and as far as Grays Harbor, Washington for the largest earthquakes on segment C. This felt shaking should also trigger evacuation, provided outreach programs have been effective. Offshore wave amplitudes for tsunamis generated by southern segment ruptures of the CSZ more than 70 km north of source areas should be somewhat smaller than the largest potential distant tsunamis and of similar or more frequent recurrence. Further work should include analysis of tsunami currents, because even 1–2-m-high tsunamis can produce strong currents that may heavily damage ports and harbors (e.g., Cherniawsky et al. 2007; Dengler et al. 2008; Wilson et al. 2012).

Acknowledgments This investigation was supported by National Oceanic and Atmospheric Administration (NOAA) Grants NA08NWS4670028 and #NA09NWS4670014. Some simulations used in this paper were conducted using computational facilities at the College of William and Mary which were provided with the assistance of the National Science Foundation, the Virginia Port Authority, and Virginia's Commonwealth Technology Research Fund, and also using the Extreme Science and Engineering Discovery Environment (XSEDE; Grant #TG-CCR120029), which is supported by National Science Foundation grant number OCI-1053575.

References

- Atwater BF, Nelson AR, Clague JJ, Carver GA, Yamaguchi DK, Bobrowsky PT, Bourgeois J, Darienzo ME, Grant WC, Hemphill-Haley E, Kelsey HM, Jacoby GC, Nishenko SP, Palmer SP, Peterson CD, Reinhart MA (1995) Summary of coastal geologic evidence for past great earthquakes at the Cascadia subduction zone. *Earthq Spectra* 11(1):1–18
- Atwater BF, Musumi-Rokkaku S, Satake K, Tsuji Y, Ueda K, Yamaguchi DK (2005) The orphan tsunami of 1700—Japanese clues to a parent earthquake in North America. *U.S. Geological Survey Professional Paper 1707*
- Blaser L, Krüger F, Ohmberger M, Scherbarum F (2010) Scaling relations of earthquake source parameter estimates with special focus on subduction environment. *Bull Seismol Soc Am* 100(6):2914–2926
- Borrero J, Dengler L, Uslu B, Synolakis C (2006) Numerical modeling of tsunami effects at marine oil terminals in San Francisco Bay, report prepared for Marine Facilities Division of the California State Lands Commission. Accessed June 2013. http://www.slc.ca.gov/Division_Pages/MFD/MOTEMS/SFTsunamiReport/SF_MOT_final_report.pdf
- Boyarko DC, Brudzinski MR (2010) Spatial and temporal patterns of nonvolcanic tremor along the southern Cascadia subduction zone. *J Geophys Res* 115(B00A22). doi:10.1029/2008JB006064
- Cherniawsky JY, Titov VV, Wang K, Li J-Y (2007) Numerical simulations of tsunami waves and currents for southern Vancouver Island. *Pure Appl Geophys* 164:465–492
- Delouis B, Nocquet J-M, Vallée M (2010) Slip distribution of the February 27, 2010 $M_w = 8.8$ Maule earthquake, central Chile, from static and high-rate GPS, InSAR, and broadband teleseismic data. *Geophys Res Lett* 37(L17305). doi:10.1029/2010GL043899
- Dengler L, Uslu B, Barberopoulou A, Borrero J, Synolakis C (2008) The vulnerability of Crescent City, California, to tsunamis generated by earthquakes in the Kuril Islands region of the northwestern Pacific. *Seismol Res Lett* 79(5):608–619. doi:10.1785/gssrl.79.5.608
- Dragert H, Hyndman RD (1995) Continuous GPS monitoring of elastic strain in the northern Cascadia subduction zone. *Geophys Res Lett* 22:755–758
- Freund LB, Barnett DM (1976) A two-dimensional analysis of surface deformation due to dip-slip faulting. *Bull Seismol Soc Am* 66:667–675
- Geist EL (1998) Local tsunamis and earthquake source parameters. In: Dmowska R, Saltzman B (eds) *Tsunamigenic earthquakes and their consequences*, *Adv Geophys* 39: 2-1–2-16
- Goldfinger C, Nelson CH et al (2003) Deep-water turbidites as Holocene earthquake proxies: the Cascadia Subduction zone and northern San Andreas fault systems. *Ann Geofis* 46(5):1169–1194

- Goldfinger C, Nelson CH, Morey A, Johnson JE, Gutierrez-Pastor J, Eriksson AT, Karabanov E, Patton J, Gracia E, Enkin R, Dallimore A, Dunhill G, Vallier T (2012) Turbidite event history: methods and implications for Holocene paleoseismicity of the Cascadia subduction zone, USGS Professional Paper 1661-F, Reston, VA, U.S. Geological Survey, 178 p., 64 figures
- González FI et al (2009) Probabilistic tsunami hazard assessment at Seaside, Oregon, for near- and far-field seismic sources. *J Geophys Res* 114(C11023). doi:[10.1029/2008JC005132](https://doi.org/10.1029/2008JC005132)
- Kelsey HM, Nelson AR, Hemphill-Haley E, Witter RC (2005) Tsunami history of an Oregon coastal lake reveals a 4600 yr record of great earthquakes on the Cascadia subduction zone. *Geol Soc Am Bull* 117:1009–1032
- Myers EP III, Baptista AM (2001) Analysis of factors influencing simulations of the 1993 Hokkaido Nansei-Oki and 1964 Alaska Tsunamis. *Nat Hazards* 23:1–28
- Nelson AR, Kelsey HM, Witter RC (2006) Great earthquakes of variable magnitude at the Cascadia subduction zone. *Quat Res* 65:354–365
- Obermeier SF, Dickenson SE (2000) Liquefaction evidence for the strength of ground motions resulting from Late Holocene Cascadia subduction earthquakes, with emphasis on the event of 1700 AD. *Bull Seismol Soc Am* 90(4):876–896
- Okada Y (1985) Surface deformation due to shear and tensile faults in a half-space. *Bull Seismol Soc Am* 75(4):1135–1154
- Priest GR, Goldfinger C, Wang K, Witter RC, Zhang Y, Baptista AM (2009) Tsunami hazard assessment of the Northern Oregon coast: a multi-deterministic approach tested at Cannon Beach, Clatsop County, Oregon. Oregon Department of Geology Mineral Industries Special Paper 41
- Priest GR, Goldfinger C, Wang K, Witter RC, Zhang Y, Baptista AM (2010) Confidence levels for tsunami-inundation limits in northern Oregon inferred from a 10,000-year history of great earthquakes at the Cascadia subduction zone. *Nat Hazards*. doi:[10.1007/s11069-009-9453-5](https://doi.org/10.1007/s11069-009-9453-5)
- Satake K, Wang K, Atwater BF (2003) Fault slip and seismic moment of the 1700 Cascadia earthquake inferred from Japanese tsunami descriptions. *J Geophys Res* 108:ESE7-1–ESE7-17
- Schatz CE, Curl H, Burt WV (1964) Tsunamis on the Oregon coast. *The Ore Bin* 26(12):231–232
- Seno T (2002) Tsunami earthquake as transient phenomena. *Geophys Res Lett* 29. doi:[10.1029/2002GL014868](https://doi.org/10.1029/2002GL014868)
- Tsuji T, Kawamura K, Kanamatsu T, Kasaya T, Fujikura K, Ito Y, Tsuru T, Kinoshita M (2013) Extension of continental crust by anelastic deformation during the 2011 Tohoku-oki earthquake: the role of extensional faulting in the generation of a great tsunami. *Earth Planet Sci Lett* 364:44–58
- US Geological Survey (2001) USGS ShakeMap: Arequipa, Peru. Accessed June 2013. <http://earthquake.usgs.gov/earthquakes/shakemap/atlas/shake/200106232033/>
- US Geological Survey (2010) USGS ShakeMap: Offshore Maule, Chile. Accessed March 2013. <http://earthquake.usgs.gov/earthquakes/shakemap/global/shake/2010ftan/>
- Wang K, He J (2008) Effects of frictional behaviour and geometry of subduction fault on coseismic seafloor deformation. *Bull Seismol Soc Am* 98(2):571–579
- Wang K, Hu Y (2006) Accretionary prisms in subduction earthquake cycles: the theory of dynamic Coulomb wedge. *J Geophys Res* 111:B06410. doi:[10.1029/2005JB004094](https://doi.org/10.1029/2005JB004094)
- Wang K, Wells R, Mazzotti S, Hyndman RD, Sagiya T (2003) A revised dislocation model of interseismic deformation of the Cascadia subduction zone. *J Geophys Res* 108(B1):2026. doi:[10.1029/2001JB001227](https://doi.org/10.1029/2001JB001227)
- Wang P-L, Engelhart SE, Wang K, Hawkes AD, Horton BP, Nelson AR, Witter RC (2013) Heterogeneous rupture in the great Cascadia earthquake of 1700 inferred from coastal subsidence estimates. *J Geophys Res Solid Earth* 118. doi:[10.1002/jgrb.50101](https://doi.org/10.1002/jgrb.50101)
- Wilson R, Davenport C, Jaffe B (2012) Sediment scour and deposition within harbors in California (USA), caused by the March 11, 2011 Tohoku-oki tsunami. *Sediment Geol* 282(C):228–240. doi:[10.1016/j.sedgeo.2012.06.001](https://doi.org/10.1016/j.sedgeo.2012.06.001)
- Witter RC (2008). Prehistoric Cascadia tsunami inundation and runup at Cannon Beach, Clatsop County, Oregon. Oregon Department of Geology Mineral Open-File Report O-08-12
- Witter RC, Zhang Y, Wang K, Priest GR, Goldfinger C, Stimely L, English JT, Ferro PA (2011) Simulating tsunami inundation at Bandon, Coos County, Oregon, using hypothetical Cascadia and Alaska earthquake scenarios. Oregon Department of Geology Mineral Industries Special Paper 43
- Witter RC, Zhang Y, Wang K, Goldfinger C, Priest GR, Allan JC (2012) Coseismic slip on the southern Cascadia megathrust implied by tsunami deposits in an Oregon lake and earthquake-triggered marine turbidites. *J Geophys Res* 117:B10303. doi:[10.1029/2012JB009404](https://doi.org/10.1029/2012JB009404)
- Zhang Y (2012) SELFIE. In: Proceedings and results of the 2011 NTHMP model benchmarking workshop, National Tsunami Hazard Mitigation Program, pp 303–336. <http://nthmp.tsunami.gov/documents/nthmpWorkshopProcMerged.pdf>. Accessed 25 Mar 2013

- Zhang Y, Baptista AM (2008) An efficient and robust tsunami model on unstructured grids Part I: inundation benchmarks. *Pure Appl Geophys* 165(11–12):2229–2248. doi:[10.1007/s00024-008-0424-7](https://doi.org/10.1007/s00024-008-0424-7)
- Zhang Y, Witter RW, Priest GP (2011) Tsunami-tide interaction in 1964 Prince William Sound tsunami. *Ocean Model* 40:246–259
- Zilkoski DB, Richards JH, Young GM (1992) Results of the general adjustment of the North American Vertical Datum of 1988. *Am Congr Surv Mapp Surv Land Inf Syst* 52(3):133–149. http://www.ngs.noaa.gov/PUBS_LIB/NAVD88/navd88report.htm. Accessed 25 Mar 2013